Delft University of Technology

Numerical analysis of noise reduction mechanisms of serrated trailing edges under zero lift condition

van der Velden, Wouter; Avallone, Francesco; Ragni, Daniele

Important note
To cite this publication, please use the final published version (if applicable).
Please check the document version above.

Numerical analysis of noise reduction mechanisms of serrated trailing edges under zero lift condition

W.C.P. van der Velden[*], F. Avallone[†] and D. Ragni[‡]

Delft University of Technology, Kluyverweg 1, 2629 HS, Delft, the Netherlands

The relation between the far-field noise and the flow field, in presence of serrated and combed-serrated trailing edge, is studied to explain the associated noise reduction mechanisms. Both serration geometries are retrofitted to a NACA 0018 wing. Computations are carried out by solving the fully explicit, transient, compressible Lattice Boltzmann equation, while the acoustic far-field is obtained by means of the Ffowcs-Williams and Hawking integral solution. A link between the far-field noise and the relevant flow parameters that contribute to noise generation is proposed. It is confirmed that the intensity of the surface pressure fluctuations varies in the streamwise direction, and that most of the low-frequency noise is generated at the root of the serrations. It is concluded that the additional noise reduction achieved by the use of combs is due to the mitigation of the outward flow motion at the root. Furthermore, it is shown that the edge-oriented correlation length and the convection velocity of the surface pressure fluctuations are the two statistical flow parameters that influence both the intensity and the frequency range of noise reduction. It is found that a larger edge-oriented correlation length contributes to noise reduction, by generating destructive interference between the pressure waves scattered along the slanted edge.

I. Introduction

Airfoil self-noise has recently become a popular problem in wind-energy. The strict regulations strongly limit the operational regimes of already installed wind-turbines, thus reducing their power production with a consequent increase of the overall cost of energy.[1]

Brooks et al.[2] identified five different physical mechanisms responsible for airfoil self-noise. In wind-turbine applications, turbulent boundary-layer trailing-edge noise is the most relevant mechanism.[3] Since trailing edge noise is determined by the scattering of the turbulent flow at the trailing edge of a blade, many passive noise-mitigation solutions have been recently developed, directed to the local modifications of the trailing-edge geometry. Several geometries have been proposed and tested.[4–6] The most popular ones are the sawtooth trailing-edge serrations, due to their simplicity of manufacturing and installation. More recently, Oerlemans[1] proposed a new geometry, named combed serration, with solid filaments in the empty spaces in between the teeth of conventional serrations. Such a design decreases the noise by additional 2 dB in the noise reduction frequency regime of interest.

Experimental measurements showed that the intensity of the noise reduction is a function of the frequency,[4, 6–12] with the largest reduction measured for the low frequency range. Many experimental investigations reported discrepancies in terms of noise reduction intensity with respect to the straight trailing-edge configuration between wind-tunnels (from 8 to 10 dB) and in-field (between 2 and 3 dB) measurements. Furthermore, a noise increase up to 5 dB was measured for frequency higher than the cross-over frequency, corresponding to a Strouhal number based on δ approximately equal to $St_\delta = f\delta/u_\infty = 1$.[4]

The reasons behind the disagreement between analytical and experimental evidence has been the object of recent investigations. Gruber et al.[4] used surface-pressure sensors to measure the pressure fluctuations along the serration surface. He concluded that serration noise reduction is due to a lower convection velocity

*PhD researcher, Faculty of Aerospace Engineering, Aerodynamics, `W.C.P.vanderVelden@TUDelft.nl`
†Post-doc, Faculty of Aerospace Engineering, Wind Energy
‡Assistant professor, Faculty of Aerospace Engineering, Wind Energy

American Institute of Aeronautics and Astronautics

(u_c) in streamwise direction, in combination with a smaller spanwise coherence (γ^2). Chong and Vathylakis[10] investigated the flow over trailing-edge serrations retrofitted to a flat plate. Their results were in disagreement with the earlier study of Gruber et al.[4] regarding the relevance of γ^2. While earlier studies on straight trailing edges concluded that a decrease of γ^2 is beneficial for noise reduction, more recent studies found that, in presence of a slanted edge, a larger γ^2 contributes to mitigate far-field noise.[12] Finally, Chong and Vathylakis[10] combined surface-pressure measurements and time-averaged surface heat-transfer measurements. They demonstrated the presence of pressure driven vortices along the serration edges, concluding that the frozen turbulence assumption is not valid in presence of a serrated trailing edge.

The effect of pressure driven vortices along the serration edge was also investigated by Arce-Leon et al.[13] and Avallone et al.[12] They experimentally demonstrated that the assumption of frozen turbulence is not valid in presence of trailing edge serrations and that the intensity of the pressure fluctuations decreases from root to tip. In particular, Avallone et al.[12] explored the link between the aerodynamic and aeroacoustic effects of serrations by using time-resolved PIV data. They estimated the right hand side of the Poisson equations[14] for the hydrodynamic pressure in proximity of the trailing edge. The authors showed that, at low frequency, noise is mainly generated at the root of the serrations, while the tip contributes more to noise generation at higher frequencies. The dominance of the root of the serration was attributed to the presence of streamwise oriented coherent structures generated by the three-dimensional mixing layer in the empty-space in between serrations even at small angles of attack.

Similar conclusions were also achieved through numerical analyses.[15–20] Jones and Sandberg[15] showed that the flow is strongly three-dimensional with the presence of horse-shoe vortices in the space between the serrations, which were promoting a seeping motion of the flow from the suction to the pressure side. van der Velden and Oerlemans[20] computed the flow around both a conventional and combed serrated trailing edge using the experiments of Arce-Leon et al.[11] as reference. They reported similar far-field noise intensity as in the reference experiments and confirmed the hypotheses of Avallone et al.[12] based on the analysis of the source term.

In the present work, the influence of serrations on the trailing edge acoustic scattering mechanisms is studied in order to understand how the design of serrations can be improved. This is obtained by addressing the link between the flow field and acoustic scattering. A conventional and a combed serration are compared in order to elucidate their noise reduction mechanisms. Both configurations are retrofitted to a NACA0018 airfoil set at zero angle of attack. A zero-lift setup is chosen to reduce the aerodynamic effects arising due to pressure differences across the serrations.[13] Computations of the flow field are carried out by solving the fully explicit, transient, compressible Lattice Boltzmann equation, while the acoustic far-field is obtained by means of the Ffowcs-Williams and Hawking integral solution.

II.   Computational method

The commercial software package Exa PowerFLOW 5.3c was used to solve the discrete Lattice-Boltzmann equations for a finite number of directions. To retrieve the Navier-Stokes relations, a third-order truncation of the ChapmanEnskog expansion can be used.[21] For a detailed description of the equations used for the source field computations the reader can refer to studies of Succi[22] and van der Velden et al.[23] Below, a summary will be provided regarding the steps taken in the overall process.

The discretization used for this particular application consists of 19 discrete velocities in three dimensions (known as the D3Q19 model). In practice this means that, a group of particles in a three-dimensional space can stream to up to 19 directions in one cell. For three dimensional simulations of low Mach number flow under ideal gas conditions, this is found to well represent the physical flow field.[22] The distribution of particles was solved using the kinetic equations on a Cartesian mesh, with the conventional Bhatnagar-Gross-Krook (BGK) collision term operator,[24] the only one available within this commercial software package. A Very Large Eddy Simulation (VLES) was implemented as viscosity model to locally adjust the numerical viscosity of the scheme in regions that are under resolved.[25] A sub-grid scale model is essential to obtain solutions of transient high Reynolds flow problems within industrial turn-around times. The model consists of a two-equation $\kappa - \epsilon$ Renormalization Group (RNG) modified to incorporate a swirl based correction that reduces the modeled turbulence in presence of large vortical structures, required for stability of the code. Due to the limitations of the discretization model D3Q19, the cells, further denoted as voxels, are equally sized in each direction. This makes it challenging to perform wall resolved simulations. Hence, a turbulent wall-model was used to resolve the near-wall region.[26] The particular choice of the wall model in combination with the

American Institute of Aeronautics and Astronautics

subgrid scale model allows to obtain a reliable estimate of the boundary layer till the viscous sub-layer, well staying within feasible turn-around times.

Due to the fact that the LBM is inherently compressible and it can only provide a time-dependent solution, the acoustic pressure field was extracted directly from the computation domain. Sufficient accuracy is obtained when considering at least 16 lattices per wavelength for the LBM methodology.[27] The obtained far field noise was further compared with noise estimated by using an acoustic analogy. For this purpose, the FW-H[28] equation was employed. The time-domain FW-H formulation developed by Farassat[29] was used to predict the far field sound radiation of the serrated trailing edge in a uniformly moving medium.[27,30] The input to the FW-H solver is the time-dependent pressure field of a porous surface mesh provided by the transient LBM simulations. A simplification was found by employing Curle's[31] analogy, where the surface mesh was fitted to the airfoil surface, commonly used in trailing edge noise predictions.

III.   Computational test-cases

A NACA 0018 airfoil with a chord of $l = 0.2$ m and span of $b = 0.08$ m ($b = 0.4l$), shown in figure 1, is investigated. The free stream velocity (u_∞) is 20 m/s, corresponding to a free stream Mach number $M_0 = 0.06$, and a chord based Reynolds number of $Re_l = 280,000$. The free stream turbulence intensity is set to 0.1% in order to replicate realistic wind tunnel conditions. The angle of attack is zero degree. The wind tunnel model and the free stream conditions are chosen as in the experiments of Arce-Leon et al.[11] The model is retrofitted with a straight, a serrated and a combed-serrated trailing edge. A sketch of the geometries together with the adopted Cartesian coordinate system is shown in figure 1. The z-axis coincides with the airfoil trailing edge; the y-axis is perpendicular to the surface of the serrations; and the x-axis is aligned with the chord of the airfoil. The origin is set at the location of the baseline airfoil straight trailing edge, such that the x-axis is oriented along the serration center-line. Serrations have length $2h = 0.04$ m ($2h = 0.2l$) and wavelength $\lambda = 0.02$ m ($\lambda = 0.1l$), resulting in an aspect ratio of $2h/\lambda = 2$. Combed serrations have the same solid geometry and filaments with both thickness and clearance of $d = 0.5$ mm ($d = 0.0025l$). Both trailing edge add-ons have the same thickness of the straight trailing edge equal to 1 mm ($t_{\mathrm{ser}} = 0.005l$). A total of 4 serrations are physically present along the span (figure 1). Transition is forced with a zig-zag strip of height $t_{\mathrm{trip}} = 0.6$ mm ($t_{\mathrm{trip}} = 0.003l$), amplitude $l_{\mathrm{trip}} = 3$ mm ($l_{\mathrm{trip}} = 0.015l$) and wavelength $b_{\mathrm{trip}} = 3$ mm ($b_{\mathrm{trip}} = 0.015l$) on both airfoil sides at $x = -0.8l$, i.e. 20% of the chord. The height of the zig-zag strip corresponds to approximately half the local incoming laminar boundary layer thickness (δ_0).

Spanwise periodic boundary conditions are applied at the edge of the model span. The simulation domain size has length equal to $12l$ in both streamwise and wall-normal directions. Outside a circular refinement zone of diameter equal to $10l$ an anechoic outer layer is used to damp-out eventually occurring acoustic reflections. A total of 10 mesh refinement regions with factor equal to 2 are employed. This guarantees that, at the trailing-edge location, the first near-wall cell is located at about $3.9 \times 10^{-4}l$, i.e. inside the viscous sub-layer. This results in a resolution of about $y^+ = 3$ around the trailing edge. The rest of the airfoil boundary is modeled with one coarser level of resolution. In total, approximately 150 million voxels are used to discretize the problem. The flow-simulation time is 0.3 seconds (30 flow passes) requiring $6,300$ CPU hours on a Linux Xeon E5-2690 2.9 GHz platform of 80 cores.

The physical time step, corresponding to a Courant-Friedrichs-Lewy (CFL) number of 1 in the finest mesh resolution level, is 1.3×10^{-7} s. The unsteady pressure on the surface of the airfoil is sampled with a frequency of 30 kHz ($St_l = fl/u_\infty = 300$) for a physical time of 0.2 s (equals to 20 airfoil flow passes), with a Hanning window size of 128 with 50 % overlap, and averaged on a 1/3rd octave band. Given the periodicity of the flow for the different serrations, the computed fields are spatially averaged along the spanwise direction, as well as over the top and bottom sides of the serration. The average is carried out along points with the same relative location with respect to the serration root. This procedure reduces the uncertainty on the mean values as well as increases the number of samples available for the spectra evaluation.[15]
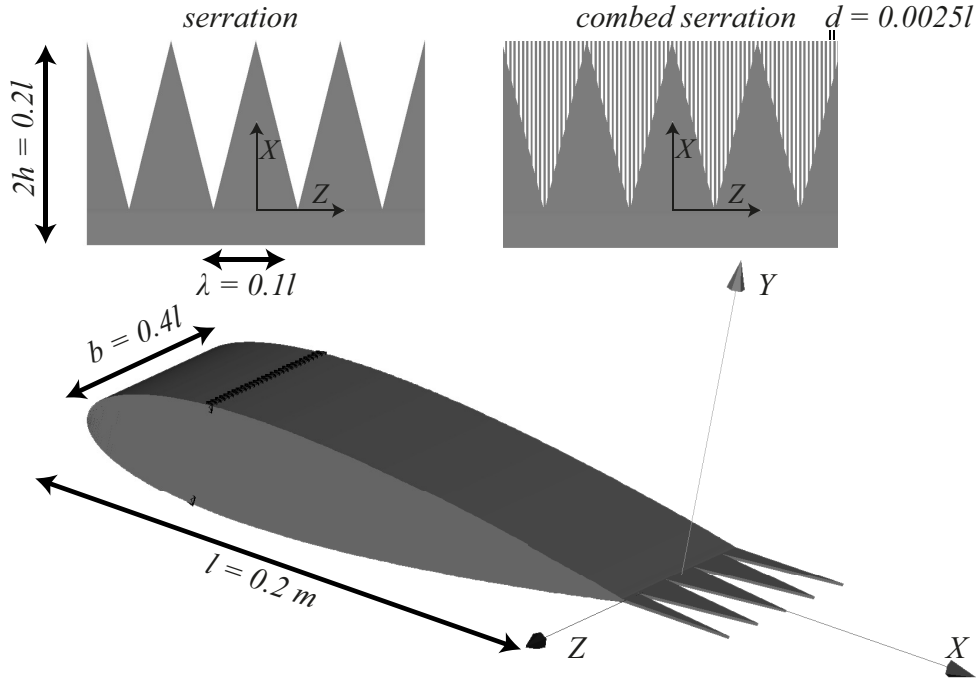
American Institute of Aeronautics and Astronautics

Figure 1. Airfoil and serration geometry and dimensions.

IV.   Far-field noise analysis

A.   Noise spectra

The far-field acoustic spectra are obtained with the FW-H analogy and compared to experimental data obtained with microphone array measurements.[11]

Far-field data (Φ_m), obtained from the FW-H integral solution method is sampled by a probe located at $x = 0, y = 10l, z = 0$, i.e. directly above the airfoil trailing edge. The reported results are scaled to a reference observer distance (R), span (b) and Mach number (M) using the following formula:

$$\Phi_{aa} = \Phi_m + 20\log_{10}(R) - 10\log_{10}(b) - 50\log_{10}(M), \tag{1}$$

where the fifth power Mach number power law has been enforced.[32–34]

The results of the calculated pressure spectrum (Φ_{aa}) as well as the corresponding noise reduction with respect to the straight trailing edge ($\Delta\Phi_{aa}$, where positive means reduction), are plotted in figure 2. The good agreement between the computational results and measurements represents a further assessment of the accuracy of the computations.

All the investigated configurations show broadband noise characteristic spectra with intensity decreasing at high frequency. It can be seen that the thin trailing-edge does not introduce any tonal component due to vortex shedding. Dilatation fields (not reported here for the sake of conciseness) also confirm that the most important noise source region is located at the trailing edge.

Both serrated trailing-edge geometries reduce noise up to $St_l = 28$ (figure 2b), corresponding to a $St_\delta = 1.35$. The maximum noise reduction is approximately equal to 7 dB and 10 dB at $St_l = 6$ for the conventional and combed serrations, respectively. The larger noise reduction for the combed serrated configuration is in agreement with experimental observations on a full-scale wind turbine.[1]
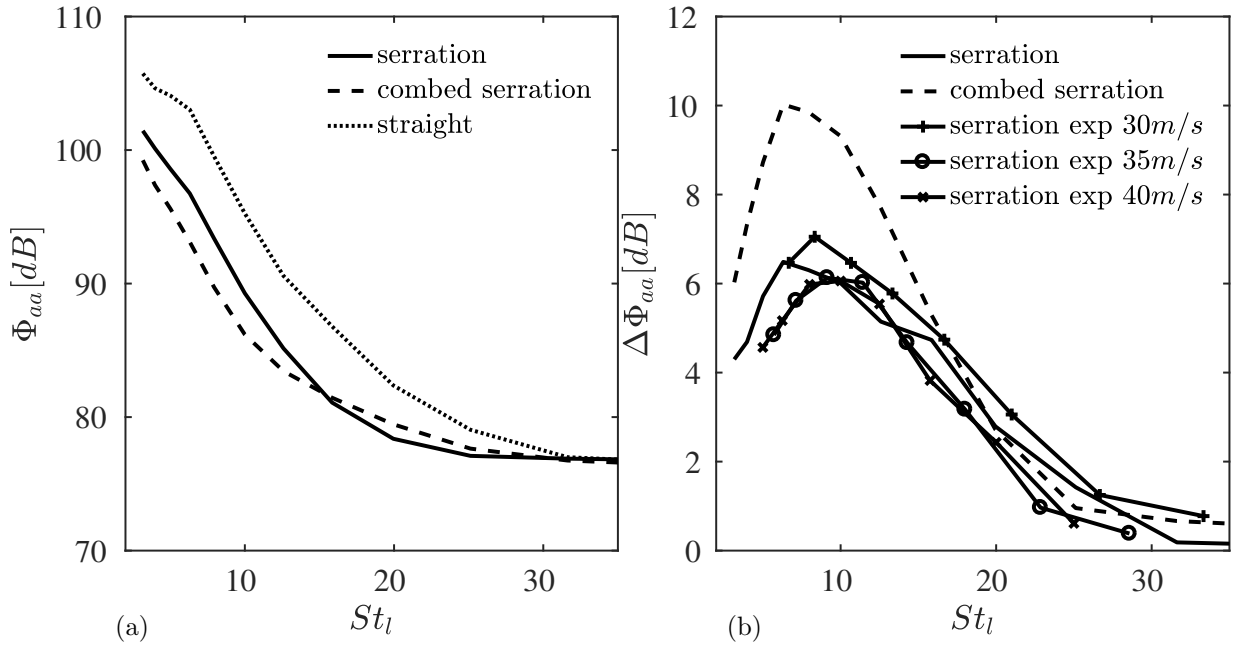
American Institute of Aeronautics and Astronautics

Figure 2. Far-field noise spectra (a) Φ_{aa} and reduction (b) $\Delta\Phi_{aa}$ with respect to the straight trailing edge model. Experimental data is taken from Arce-Leon et al.[11]

B. Noise directivity

The far-field pressure fluctuations are further used to compute directivity plots, to assess the reproducibility of the dipole characteristics of trailing-edge noise. In this section, noise directivity plots are obtained by placing 360 pressure probes in a circle of diameter equal to $10l$ at the airfoil mid-span. Results are plotted for three different frequency bands in figure 3.

As expected, a coupled dipole radiation pattern is observed in the low frequency range, corresponding to a ratio of acoustic wavelength to airfoil chord of 4. At higher frequencies, the directivity pattern becomes asymmetric with respect to the streamwise direction, with higher noise levels towards the leading edge due to the phase shift of the acoustic pressure from both airfoil sides.[35] In this respect, it can be seen that the acoustic waves from both airfoil sides destructively interfere upstream of the leading edge, thus creating a zone of silence. In the range of the highest Strouhal numbers, a non-compact behavior is observed.

Around $2 < St_l < 16$, the presence of the add-ons results in noise reduction in all directions. The largest reduction is observed at upstream angles between $105 - 135$ degrees. At higher frequencies, differences between the serrated and combed-serrated configurations are negligible. From the plots, it can be deduced that the upstream traveling waves are more effectively canceled out with the trailing-edge devices, affecting the overall directivity pattern.

C. Chord-wise strip FW-H analysis

In the previous section, it was shown that the combed serrated geometry outperforms the conventional geometry by additional reducing noise up to 3 dB. This section covers a detailed analysis of the acoustic data to assess the working mechanisms of serrations. Most of the earlier studies presented in the introduction have been pointed out the importance of the wall pressure fluctuations from both a hydrodynamic point and an acoustic feedback points of view. The location and directivity of the scattered pressure waves however, were often neglected. The study on how the scattered pressure waves interfere with each other however, becomes extremely relevant, especially within the target of explaining the dependence of the noise reduction upon its frequency.

Both airfoil and serrations are split into segments as shown in figure 4. Each segment is independently used to compute the pressure fluctuations in the far-field. The methodology allows creating a link between the scattering at the edge and the far-field constructive/destructive interference for different streamwise locations along the slanted edge (e.g. the root region, the tip one). In this study, 9 segments are considered
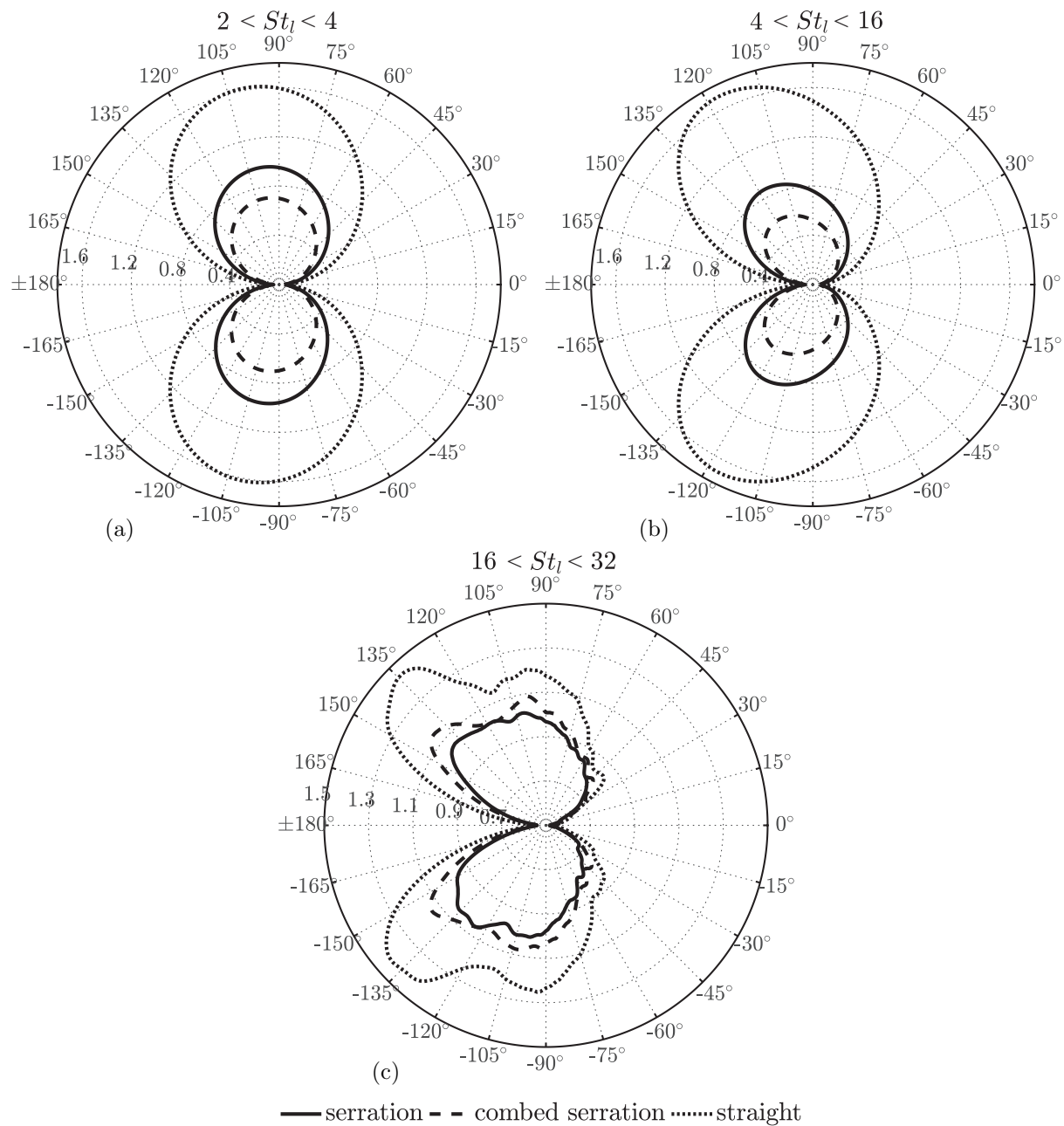
American Institute of Aeronautics and Astronautics

Figure 3. Directivity plot of $\Phi_{aa}(\alpha, \Delta f)/\Phi_{aa}(\Delta f)$ for the straight, serrated and combed serrated trailing edge models under different Strouhal numbers. (a) $2 < St_l < 4$, (b) $4 < St_l < 16$ and (c) $16 < St_l < 32$. Normalized by mean values of the straight edge case.

American Institute of Aeronautics and Astronautics

to cover the last 5% of the airfoil chord, as well as the entire serration. The segments are numbered from 1 to 9 from the root to the tip, while the entire region is indicated with 0 (figure 4). The FW-H analogy is then applied for the cumulative sum of segments (e.g. $1-2, 1-3,...$). Results from each segment allow detecting the interference location, while the cumulative sum allow quantifying the constructive and destructive interference.

The cumulative sum of segments is plotted in figure 4 for both the serrated (a) and combed serrated (b) trailing edges. Three different frequency ranges are considered. The values are compared with respect to the far-field spectra of the overall region, Φ_{aa}^0. Positive values of $\Phi_{aa}^\# - \Phi_{aa}^0$ indicate that the noise generated by the partial sum of segments is larger than the noise generated by the entire serration. Different growth rates denote different distributions of sources along the serration for different ranges of frequency. For $2 < St_l < 4$, both configurations show a local maximum for the cumulative sum at segment $1-4$. In this frequency range, the noise intensity generated near the root is larger than the one of the overall airfoil, thus confirming that this location is mostly contributing to the overall scattered noise.[12] Adding more segments, a reduction is observed. The result evidences the destructive interference between the pressure waves scattered at the root and at the mid/tip regions. One major observation concerns the different behavior between serrated and combed serrated trailing edges: while they both show similar trends up to segment 6, they are different near the tip. The serrated trailing edge shows a converged result, while the combed serrated model still shows increasing intensity.
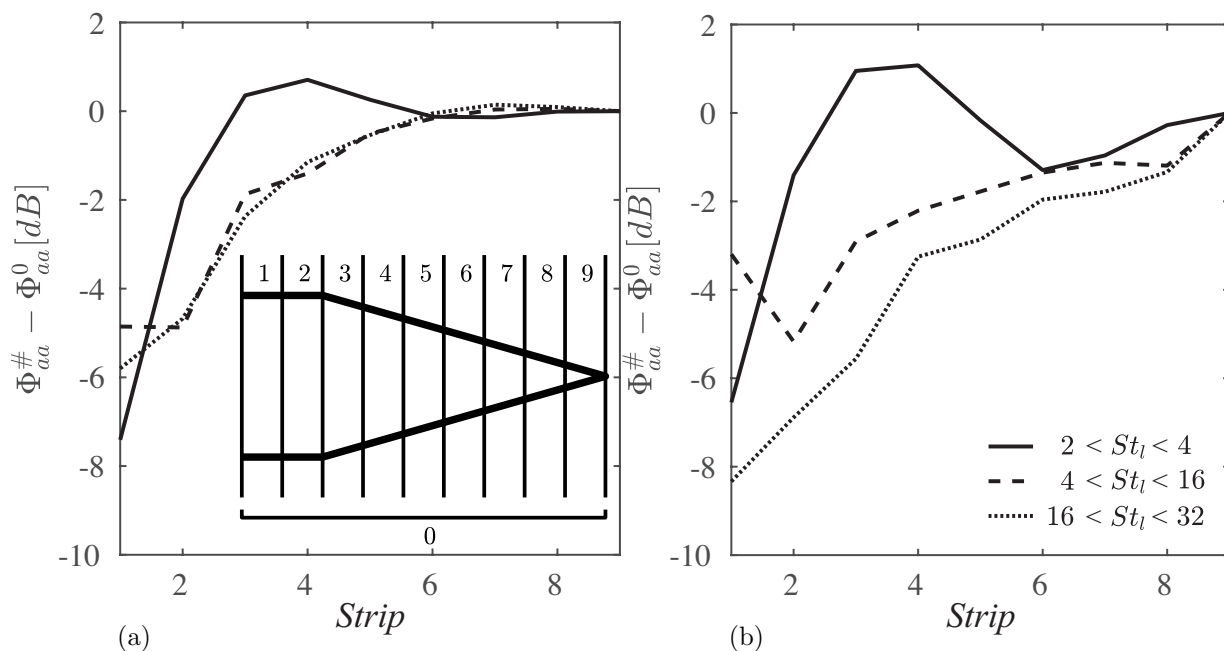

Figure 4. Cumulative sum of far-field sound pressure levels from root to tip (segment 1, $1-2$, $1-3$, ...) for the serration (a) and combed serration (b).

At higher Strouhal numbers, no local-maxima are found in the cumulative procedure, but the largest contributions are encountered towards the tip. The serrated trailing edge does not show any relevant difference for the frequency ranges $4 < St_l < 16$ and $16 < St_l < 32$, while for the combed serrated trailing edge, the intensity decreases at higher frequencies.

Summarizing, the introduction of the combs:

- alters the distribution of the noise sources along the slanted edge thus causing destructive interference in the far-field. More specifically, they mitigate the noise generated at the root (i.e., mitigation of the pressure fluctuations created by the sudden interaction between pressure and suction side);

- increases the contribution of the acoustic sources generated at the tip. However, as it will be shown later in section A, the intensity of the pressure fluctuations at the tip is typically lower than at the root.

American Institute of Aeronautics and Astronautics

V. Effect of serrations on the flow field

The near-wall spatial distributions of the time-averaged mean velocity components are shown in figure 5 and figure 6 for the serrated and the combed-serrated geometry, respectively. Data is extracted on a plane close to the surface, i.e. $y/\delta = 0.05$ ($y = 0.5$ mm) and averaged and mirrored as discussed in section III. They are plotted at this location such that can be compared with previous literature.[11, 12, 15] In presence of a serrated trailing edge, the mean streamwise velocity component increases from the root to the tip, corresponding to an acceleration of the flow with a thinning effect of the boundary layer.[12] The flow tends to seep into the empty space in between serrations (downward motion) as evidenced by the negative mean wall-normal velocity component ($\overline{v}$). As a direct consequence, the flow exhibits an outward motion as visible from the spanwise velocity component ($\overline{w}$). Differently, in presence of combed serrations, where the streamwise component ($\overline{u}$) shows similar flow features, the downward motion of the wall normal velocity ($\overline{v}$) at the edge of the solid part of the serration is weaker. Furthermore, the spanwise component ($\overline{w}$) is approximately zero because of the presence of the combs that align the flow. In the same figure, the mean flow direction in the $x-z$ plane ($\tan^{-1}(\overline{u},\overline{w})$) is plotted for a better visualization. Flow alignment positively contributes to noise reduction as stated by Howe[36] and Chong and Vathylakis.[10] However, it has been shown that this curvature effect is not the only driving mechanism to justify the mis-prediction from literature.[11]
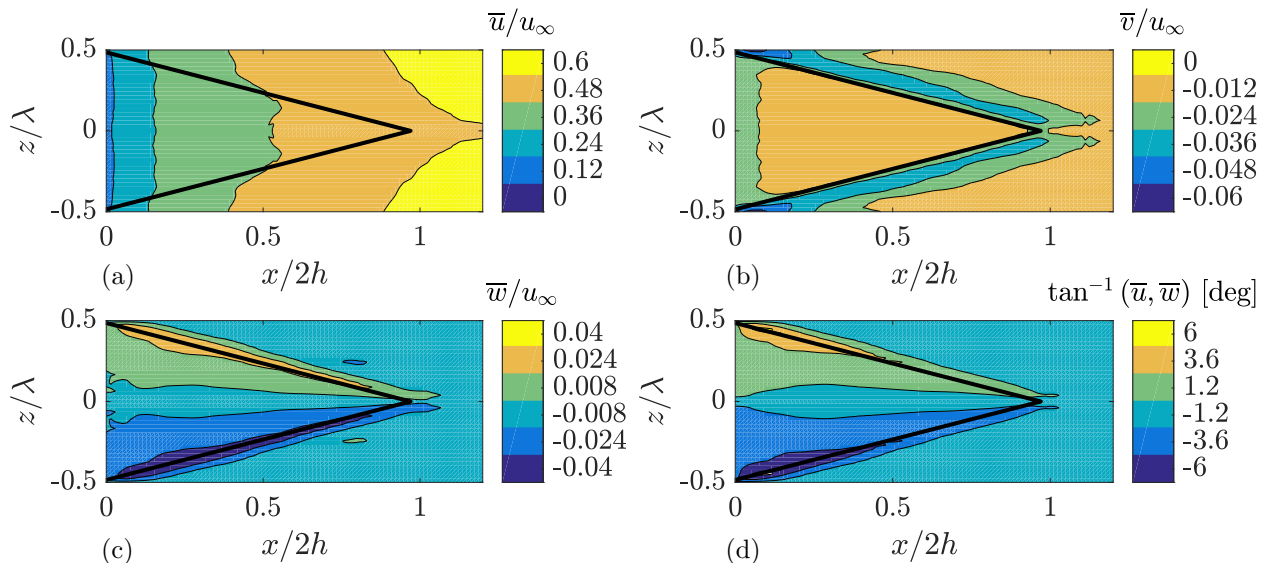

Figure 5. Contour of the mean velocity component over the serration at $y/\delta = 0.05$: (a) streamwise, $\overline{u}$, (b) wall-normal, $\overline{v}$, (c) spanwise, $\overline{w}$ velocity components and (d) stream and spanwise angle, $\tan^{-1}(\overline{u},\overline{w})$. Projections of the solid serration on the $x-z$ plane are indicated by means of continuous black lines.

VI. Surface pressure characteristics

A. Mean surface pressure fluctuations

The far-field noise is generated by the scattering of the surface pressure fluctuations at the trailing edge. To further understand the fundamental mechanisms of trailing edge serrations, a statistical analysis is carried out. Time-averaged surface pressure fluctuations ($\overline{p'p'}$) are plotted in figure 7. Results clearly show that the spatial distribution and the intensity of the surface pressure fluctuations are similar for both configurations. Additionally, the intensity of the time-averaged surface pressure fluctuations is a strong function of the streamwise location, and a weak one of the spanwise direction. The intensity decreases from root to tip by a factor two, suggesting a streamwise varying intensity of the scattered pressure waves[12] which is confirming the aforementioned observations from the FW-H strip analysis. The streamwise intensity variation of the pressure fluctuations can be caused by the flow deviation due to the fact that serrations are aligned with the chord of the airfoil. This assumption is supported by the mean wall-normal velocity components shown in figure 5 and figure 6, where $\overline{v}$ unequal to zero is measured for both configurations at $0 < x/2h < 0.1$.
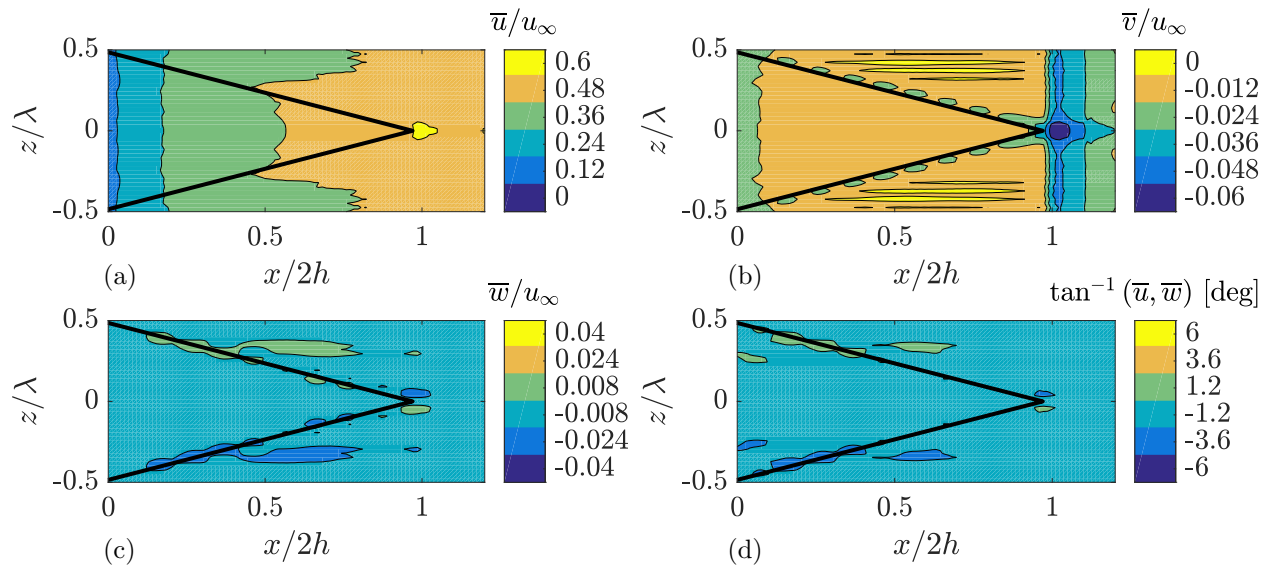
American Institute of Aeronautics and Astronautics

Figure 6. Contour of the mean velocity component over the combed serration at $y/\delta = 0.05$: (a) streamwise, $\overline{u}$, (b) wall-normal, $\overline{v}$, (c) spanwise, $\overline{w}$ velocity components and (d) stream and spanwise angle, $\tan^{-1}(\overline{u}, \overline{w})$. Projections of the solid serration on the $x - z$ plane are indicated by means of continuous black lines.
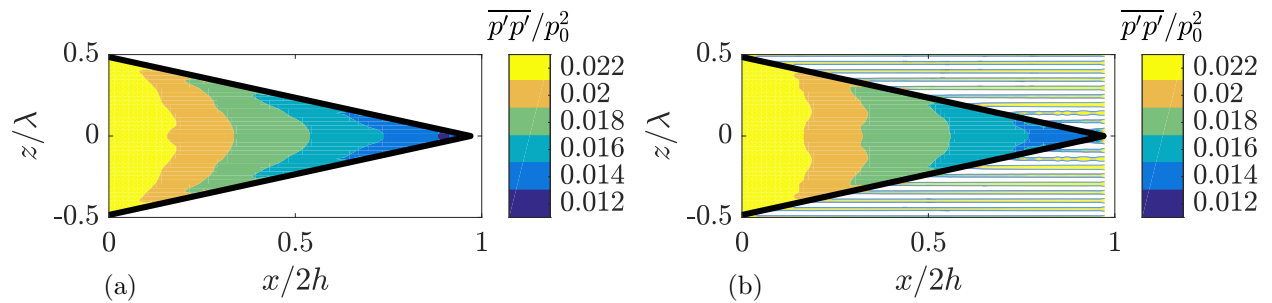

Figure 7. Intensity of the mean surface pressure fluctuation ($\overline{p'p'}/p_0^2$): (a) serration and (b) combed serration. The serration edge in the $x - z$ plane is indicated by means of continuous black lines.

The fact that $\overline{p'p'}$ does not significantly depend upon the serration geometry suggests that the reduced far-field noise generated in presence of the combed serrated geometry (as shown earlier in figure 2b) is mainly due to a different interference mechanism along the edge rather then globally different integrated fluctuation levels. This is confirmed by the observation that spectra of the pressure fluctuations at different locations along the edge are only weakly sensitive to the different geometry, as plotted in figure 8. Three reference points along the edge of the serrations at $x/2h = 0$, 0.5 and 1 are considered. The intensity of Φ_{pp} is slightly larger (approximately 2 dB) for the combed serrated geometry in the low frequency range ($5 < St_l < 10$). At the root location, spectra of the baseline configuration are similar to both the serrated configurations. A deeper analysis of the figure suggests that noise reduction benefits of the streamwise variation of Φ_{pp}. In order to better explain this effect, $\Delta\Phi_{pp} = \Phi_{pp}^{root} - \Phi_{pp}^{x}$, where Φ_{pp}^{root} and Φ_{pp}^{x} are the power spectra intensity at the root location and at the other streamwise points is plotted in figure 8b. In the frequency range where the $\Delta\Phi_{pp} > 0$, far-field noise reduction is measured, implying that a split plate on itself would also reduce noise.
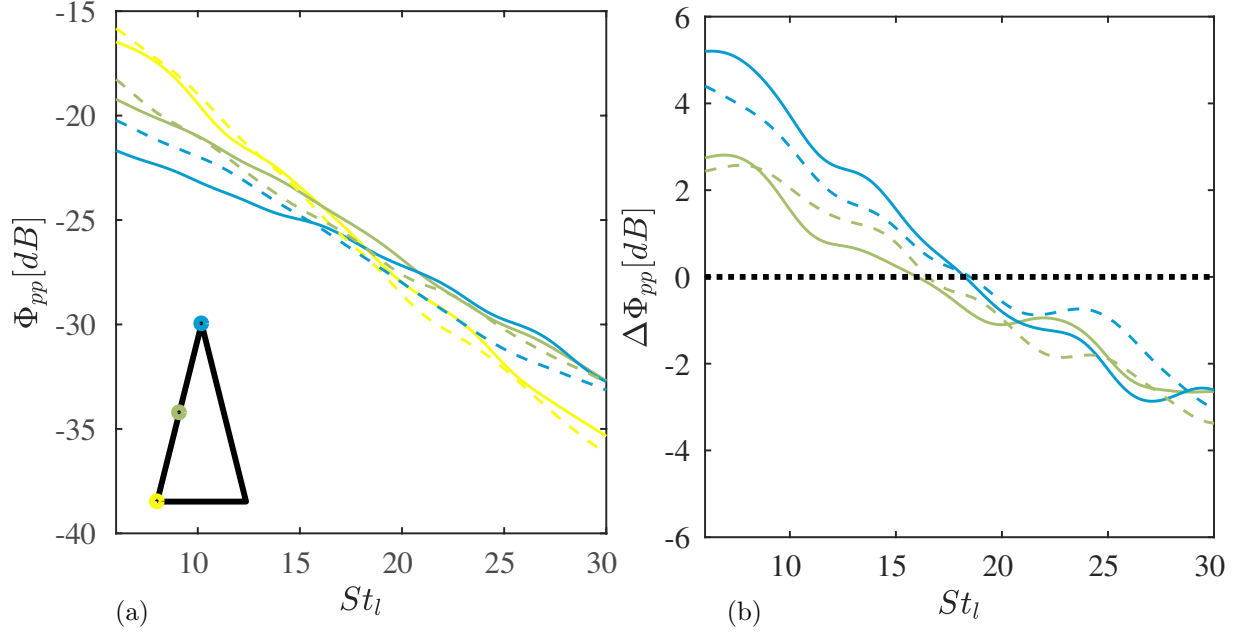

Figure 8. (a) Spectra of the surface pressure fluctuations (Φ_{pp}) at three streamwise locations corresponding to $x/2h = 0$ (yellow), 0.5 (green) and 1 (blue). The continuous and dashed lines represent the serration and combed serration respectively. (b) $\Delta\Phi_{pp} = \Phi_{pp}^{root} - \Phi_{pp}^{stream}$ with respect to the root location.

B.   Correlation length

A relevant parameter for turbulent boundary layer trailing edge noise is the spanwise correlation length (l_z).[14] It can be seen as the length of a source term scattering at the edge. Due to the modified trailing edge geometry, the correlation is estimated along the edge instead, following Kim et al.,[18] and it will be referred to as edge correlation length (l_{ze}, figure 9b):

$$l_{ze} = \int_{\infty}^{\infty} \sqrt{\gamma^2(x_e, z_e, 0, \Delta e)}\, de \tag{2}$$

where γ^2 is the magnitude-square-coherence evaluated along the edge. It is computed with a periodogram approach using Hanning windows. In order to improve convergence, data are spatially averaged over all the serrations present in the computational domain as discussed above. The resulting frequency resolution is equal to 300 Hz.

The integral limits on the mid position of the serration are chosen to visualize the asymmetry of γ^2 due to flow variations in the streamwise direction. The reference point is selected at half of the serration length ($x/2h = 0.5$) for the serrated case and at the mid-plane ($z = 0$) for the straight case. It has been

American Institute of Aeronautics and Astronautics

verified that, as expected for turbulent flows, γ^2 monotonically decreases with edge separation regardless of the reference location, as also reported by Chong and Vathylakis.[10] The fact that the coherence function approaches zero for the three investigated configurations is a proof of the convergence of the integral and it allows for cross-comparison of the simulations.

The integrated edge correlation length versus the chord based Strouhal number is shown in figure 9. l_{ze} is larger for both the conventional and combed serrations with respect to the straight configuration. According to Amiet citeamiet and Moreau and Roger,[37] in presence of a straight trailing edge, far-field noise increases in presence of larger spanwise correlation length. An opposite trend is measured in the current dataset. This result however, is in agreement with the spanwise correlation length based on the experimental spanwise velocity component (w) reported by Avallone et al.,[12] Arce-Leon et al.[13] and van der Velden and Oerlemans.[20] Physically, the larger correlation length at low St_l is caused by the formation of edge oriented vortices due to the shear layer between the solid surface and the empty space in between serrations.[38,39] It can simply be explained by the streamwise convection effect, which is the dominant effect in the slanted edge. Due to the fact that the coherence scales with the size of the vortices, and that the filtering in frequency acts as a scale separation,[40] the edge correlation length is increased.
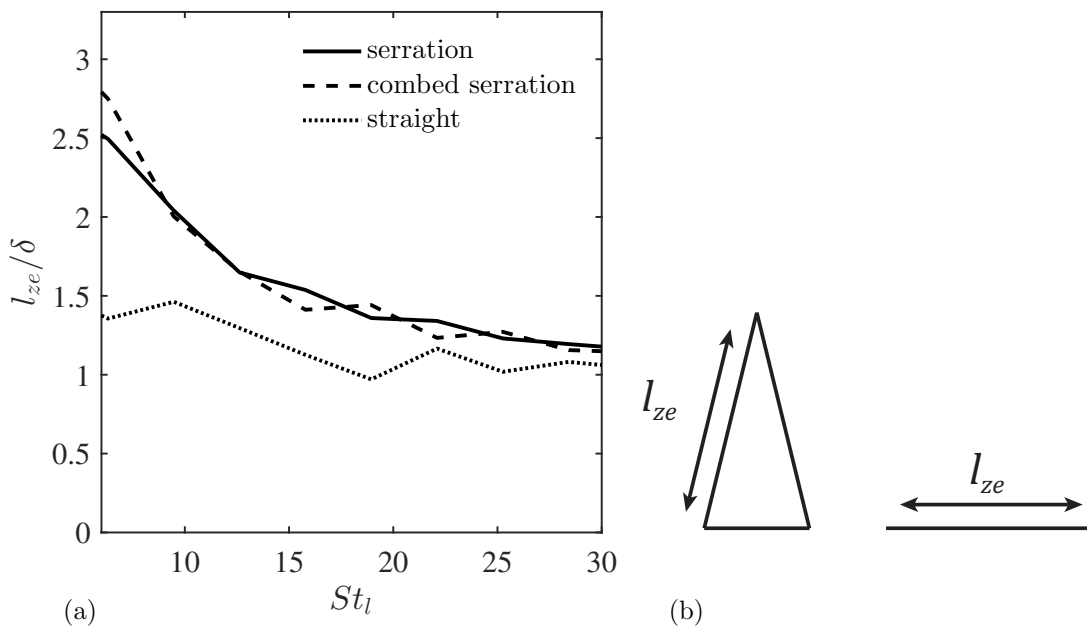

Figure 9. (a) Edge correlation length (l_{ze}) versus the Strouhal number based on the chord (St_l). (b) Sketch representing the edge correlation length for the serrated and straight trailing edge.

The presence of the combs reduces the flow-discontinuity at the edge thus resulting in a larger correlation length. l_{ze} decreases at higher frequencies with larger slope when noise reduction add-ons are installed. The difference in edge correlation length becomes less relevant from $St_l > 28$, where far-field noise reduction tends to zero. It suggests that small structures are less affected by the modification of the geometry.

However, following the conclusions of Lyu et al.,[41] a larger correlation length may be beneficial in presence of a slanted edge. It may cause destructive interference because of the phase difference between scattered pressure waves within a spanwise correlation length.[41] This conclusion is in line with the results presented earlier by the acoustic far-field segmentation study (see section C), and it physically explains the larger noise reductions observed by combed serrations.

C.   Convection velocity analysis

The flow alteration due to the serration geometry and the presence of the three-dimensional mixing layer induces spanwise motion as shown by the mean flow features in section V. Arce-Leon et al.[13] showed that it is not possible to predict the correct far-field noise by applying Howe's theory with the corrected direction of the flow at the edge. However, they did not consider the fact that the distorted flow at the edge influences the convective velocity. For this reason, the convective velocity of the surface pressure fluctuations in the

American Institute of Aeronautics and Astronautics

streamwise direction (u_c) is computed for all the points along the edge. Since the far-field noise reduction is a function of frequency, u_c is computed following a spectral approach:[10, 42, 43]

$$u_c(x, z, f) = 2\pi \Delta x \left(\frac{\partial \phi}{\partial f} \right)^{-1} \tag{3}$$

where ϕ is the phase angle obtained from the CSD between adjacent cells in the streamwise direction (figure 10b). In the following, results are averaged along the entire edge in order to easily compare the serrated case with the straight trailing edge.[18]

The convective velocity averaged along the edge per St_l is plotted in figure 10a. Even if not plotted here, it is verified that the frequency averaged convective velocity increases from the root to the tip of the serration, in agreement with previous studies.[11, 12, 19] As expected, for all the configurations under investigation, the edge-average streamwise u_c decreases with increasing St_l, since smaller eddies are convected closer to the wall. Furthermore, the convective velocity is larger for the straight trailing edge, while it is lower for the serrated cases. In the frequency range $18 < St_l < 25$, an opposite trend is measured. At frequency $St_l > 25$, the calculation of the u_c is affected by numerical noise. Comparing this result with the far-field noise it is evident that a lower convective velocity is beneficial to noise reduction. However, the difference in the noise mitigation efficiency of the two serrated geometries cannot be inferred to a different u_c.
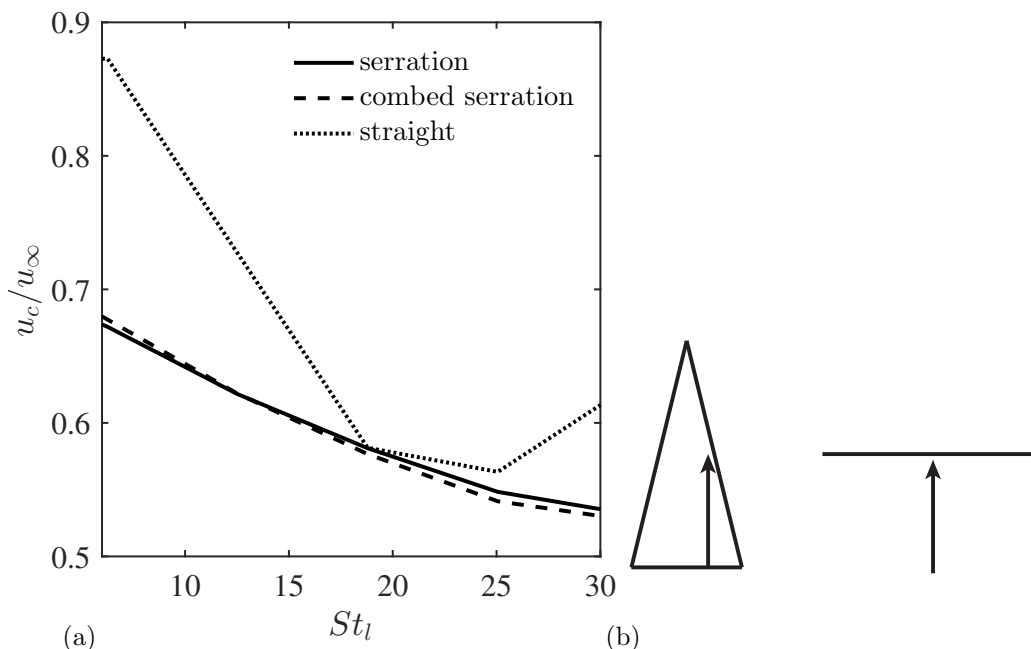

Figure 10. (a) Convective velocity (u_c) versus the Strouhal number based on the chord (St_l). (b) Sketch representative of the points used to compute the phase angle in the streamwise direction.

VII. Conclusions

The turbulent flow over a NACA 0018 airfoil with and without trailing edge serrations and the resulting scattered turbulent boundary-layer trailing-edge noise were investigated, aiming at explaining the noise reduction mechanisms of these trailing-edge add-ons. The flow field was computed by solving the fully explicit, transient, compressible Lattice Boltzmann equations, while the acoustic far-field was obtained by means of the Ffowcs-Williams and Hawking integral solution. Both conventional serrated and comb serrated trailing-edge add-ons were compared with the straight trailing-edge configuration. It was shown that the combed serrations give a larger noise reduction than the conventional serration.[1]

The intensity of the time-averaged surface pressure fluctuations on the serrated surface were found to decrease in streamwise direction and only weakly depending on the serration geometry. Using the chord-wise FW-H strip analysis, the trailing edge was further split in different segments from which the corresponding

American Institute of Aeronautics and Astronautics

far-field noise was computed by means of the FW-H analogy. The combed serrated geometry altered the distribution of the noise sources, both in space and frequency, by reducing the noise sources at the root. The distribution of the noise sources is such that they led to destructive interference in the far-field.

Aiming at detecting the physical parameters that contribute to noise generation, the space and time correlations of the surface pressure fluctuations were further investigated. It was demonstrated that the most relevant parameters that can be tuned in order to control the intensity and the frequency range of the noise reduction were the edge-oriented correlation length (l_{ze}) and the convection velocity ($u_c/\cos(\beta)$) along the edge.

It was observed that the edge-oriented correlation length increases with a slanted edge, with the largest correlation length found for the combed-serrated trailing edge. It can simply be explained by the streamwise convection effect, which is the dominant effect in the slanted edge. It causes destructive interference because of the phase difference between scattered pressure waves within a spanwise correlation. On the other hand, the largest convection velocity over the entire frequency range was found in presence of the straight trailing edge, making it evident that a lower convective velocity is beneficial to noise reduction.

Acknowledgments

References

[1] Oerlemans, S., "Reduction of wind turbine noise using blade trailing edge devices," *22nd AIAA/CEAS Aeroacoustics Conference*, , No. 3018, 2016.

[2] Brooks, T., Pope, D., and Marcolini, M., "Airfoil self-noise and prediction," Tech. rep., NASA Reference Publication 1218, 1989.

[3] Wagner, S., Bareiss, R., and Guidati, G., *Wind Turbine Noise*, Springer, 1996.

[4] Gruber, M., Joseph, P., and Azarpeyvand, M., "An experimental investigation of novel trailing edge geometries on airfoil trailing edge noise reduction," *19th AIAA/CEAS Aeroacoustic Conference*, , No. 2011, 2013.

[5] Azarpeyvand, M., Gruber, M., and Joseph, P., "An analytical investigation of trailing edge noise reduction using novel serrations," *19th AIAA/CEAS Aeroacoustic Conference*, , No. 2009, 2013.

[6] Arce-León, C., Avallone, F., Ragni, D., and Pröbsting, S., "PIV investigation of the flow past solid and slitted sawtooth serrated trailing edges," *54th AIAA Aerospace Sciences Meeting*, , No. 1014, 2016.

[7] Dassen, A., Parchen, R., Bruggeman, J., and Hagg, F., "Results of a wind tunnel study on the reduction of airfoil self-noise by the application of serrated blade trailing edges," *Proceeding of the European Union Wind Energy Conference and Exhibition*, 1996, pp. 800–803.

[8] Oerlemans, S., Sijtsma, P., and Lopez, B. M., "Reduction of wind turbine noise using optimized aifoils and trailing-edge serrations," *AIAA Journal*, Vol. 47, 2009, pp. 1470–1481.

[9] Parchen, R., Hoffmans, W., Gordner, A., and Braun, K., "Reduction of airfoil self-noise at low Mach number with a serrated trailing edge," *International Congress on Sound and Vibration*, 1999, pp. 3433–3440.

[10] Chong, T. and Vathylakis, A., "On the aeroacoustic and flow structures developed on a flat plate with a serrated sawtooth trailing edge," *Journal of Sound and Vibration*, Vol. 354, 2015, pp. 65–90.

[11] Arce-León, C., Merino-Martínez, R., Ragni, D., Avallone, F., and Snellen, M., "Boundary layer characterization and acoustic measurements of flow-aligned trailing edge serrations," *Experiments in Fluids*, Vol. 57, No. 182, 2016.

[12] Avallone, F., Pröbsting, S., and Ragni, D., "Three-dimensional flow field over a trailing-edge serration and implications on broadband noise," *Physics of Fluids*, Vol. 28, 2016, pp. 1–20.

[13] Arce-León, C., Ragni, D., Pröbsting, S., Scarano, F., and Madsen, J., "Flow topology and acoustic emissions of trailing edge serrations at incidence," *Experiments in Fluids*, Vol. 57, No. 91, 2016.

[14] Stalnov, O., Chaitanya, P., and Joseph, P., "Towards a non-empirical trailing edge noise prediction model," *Journal of Sound and Vibration*, Vol. 372, 2016, pp. 50–68.

[15] Jones, L. and Sandberg, R., "Acoustic and hydrodynamic analysis of the flow around an aerofoil with trailing edge serrations," *Journal of Fluid Mechanics*, Vol. 706, 2012, pp. 295–322.

[16] Arina, R., Rinaldi, R. D. R., Iob, A., and Torzo, D., "Numerical study of self-noise produced by an airfoil with trailing-edge serrations," *18th AIAA/CEAS Aeroacoustic Conference*, , No. 2184, 2012.

[17] Sanjose, M., Meon, C., Masson, V., and Moreau, S., "Direct numerical simulation of acoustic reduction using serrated trailing-edge on an isolated airfoil," *20th AIAA/CEAS Aeroacoustics Conference*, , No. 2324, 2014, pp. 1–15.

[18] Kim, J., Haeri, S., and Joseph, P., "On the reduction of aerofoil-turbulence interaction noise associated with wavy leading edges," *Journal of Fluid Mechanics*, Vol. 792, 2016, pp. 526–552.

[19] van der Velden, W., van Zuijlen, A., and Ragni, D., "Flow topology and noise emission around straight, serrated and slitted trailing edges using the Lattice Boltzmann methodology," *22nd AIAA/CEAS Aeroacoustics Conference*, , No. 3021, 2016.

[20]van der Velden, W. and Oerlemans, S., "Numerical analysis of noise reduction mechanisms on improved trailing edge serrations using the Lattice Boltzmann method," *35th ASME Wind Energy Symposium*, 2017, pp. 1–15.

[21]Chen, H., Chen, S., and Matthaeus, W., "Recovery of the Navier-Stokes equations using a lattice-gas Boltzmann method," *Physical Review*, Vol. 8, No. 5339-5342, 45.

[22]Succi, S., *The lattice Boltzmann equation for fluid dynamics and beyond*, Oxford University Press, 2001.

[23]van der Velden, W., *Computational aeroacoustic approaches for wind turbine blade noise prediction*, Ph.D. thesis, Delft University of Technology, 2017.

[24]Bhatnagar, P., Gross, E., and Krook, M., "A model for collision processes in gases: Small amplitude processes in charged and neutral one-component systems," *Physical Review*, Vol. 94, No. 3, 1954, pp. 511–525.

[25]Yakhot, V. and Orszag, S., "Renormalization group analysis of turbulence. I Basic theory," *Journal of Scientific Computing*, Vol. 1, No. 1, 1986, pp. 3–51.

[26]Launder, B. and Spalding, D., "The numerical computation of turbulent flows," *Computer Methods in Applied Mechanics and Engineering*, Vol. 3, 1974, pp. 269–289.

[27]Bres, G., Perot, F., and Freed, D., "Properties of the Lattice-Boltzmann method for acoustics," *15th AIAA/CEAS Aeroacoustic Conference*, Vol. 3711, 2009, pp. 1–14.

[28]Ffowcs-Williams, J. and Hawkings, D., "Sound generation by turbulence and surfaces in arbitrary motion," *Philosophical Transactions of the Royal Society of London*, Vol. 264, 1969, pp. 321–342.

[29]Farassat, F. and Succi, G., "A review of propeller discrete frequency noise prediction technology with emphasis on two current methods for time domain calculations," *Journal of Sound and Vibration*, Vol. 71, No. 3, 1980, pp. 399–419.

[30]Casalino, D., "An advanced time approach for acoustic analogy predictions," *Journal of Sound and Vibration*, Vol. 261, No. 4, 2003, pp. 583–612.

[31]Curle, N., "The influence of solid boundaries upon aerodynamic sound," *Proceedings of the Royal Society of London*, Vol. 231, 1955, pp. 505–514.

[32]Ffowcs-Williams, J., "Hydrodynamic Noise," *Annual Review of Fluid Mechanics*, Vol. 1, 1969, pp. 197–222.

[33]Költzsch, P., *Strömungsmechanisch erzeugter Lärm*, Ph.D. thesis, Technische Universität Dresden, 1974.

[34]Blake, W., *Mechanics of flow-induced sound and vibration, volumes I and II*, Academic Press, 1986.

[35]Roger, M. and Moreau, S., "Extensions and limitations of analytical airfoil broadband noise models," *International Journal of Aeroacoustics*, Vol. 9, No. 3, 2010, pp. 273–305.

[36]Howe, M., "Aerodynamic noise of a serrated trailing edge," *Journal of Fluids and Structures*, Vol. 5, 1991, pp. 33–45.

[37]Moreau, S. and Roger, M., "Back-scattering correction and further extensions of Amiet's trailing-edge noise model. Part II: Application," *Journal of Sound and Vibration*, Vol. 323, 2009, pp. 397–425.

[38]Wygnanski, I., Tewes, P., Kurz, H., Taubert, L., and Chen, C., "The application of boundary layer independence principle to three-dimensional turbulent mixing layers," *Journal of Fluid Mechanics*, Vol. 675, 2011, pp. 336–46.

[39]Wlezien, R. and Kibens, V., "Passive control of jets with indeterminate origins," *AIAA Journal*, 1986, pp. 1263–70.

[40]Corcos, G., "The structure of the turbulent pressure field in boundary layer flows," *Journal of Fluid Mechanics*, Vol. 18, No. 3, 1964, pp. 353–378.

[41]Lyu, B., Azarpeyvand, M., and Sinayoko, S., "Prediction of noise from serrated trailing edges," *Journal of Fluid Mechanics*, Vol. 793, 2016, pp. 556–588.

[42]Panton, R. and Robert, G., "The Wavenumber-Phase Velocity Representation for the Turbulent Wall-Pressure Spectrum," *Journal of Fluids Engineering*, Vol. 116, No. 477, 1994.

[43]Romano, G., "Analysis of two-point velocity measurements in near-wall flows," *Experiments in Fluids*, Vol. 20, 1995, pp. 68–83.